

Phonon pressure coefficients and deformation potentials of wurtzite AlN determined by uniaxial pressure-dependent Raman measurements

G. Callsen,^{*} M. R. Wagner, J. S. Reparaz, F. Nippert, T. Kure, S. Kalinowski, and A. Hoffmann
Institut für Festkörperphysik, Technische Universität Berlin, Hardenbergstr. 36, 10623 Berlin, Germany

M. J. Ford and M. R. Phillips

Department of Physics and Advanced Materials, University of Technology Sydney, P.O. Box 123, Broadway, New South Wales 2007, Australia

R. F. Dalmau and R. Schlessler

HexaTech, Inc., 991 Aviation Pkwy, Morrisville, North Carolina 27560, USA

R. Collazo and Z. Sitar

Material Science and Engineering, North Carolina State University, Raleigh, North Carolina, USA

(Received 14 March 2014; revised manuscript received 13 October 2014; published 7 November 2014)

We studied bulk crystals of wurtzite AlN by means of uniaxial pressure-dependent Raman measurements. As a result, we derive the phonon pressure coefficients and deformation potentials for all zone center optical phonon modes. For the A_1 and E_1 modes, we further experimentally determined the uniaxial pressure dependence of their longitudinal optical–transverse optical (LO–TO) splittings. Our experimental approach delivers new insight into the large variance among previously reported phonon deformation potentials, which are predominantly based on heteroepitaxial growth of AlN and the ball-on-ring technique. Additionally, the measured phonon pressure coefficients are compared to their theoretical counterparts obtained by density functional theory implemented in the SIESTA package. Generally, we observe a good agreement between the calculated and measured phonon pressure coefficients but some particular Raman modes exhibit significant discrepancies similar to the case of wurtzite GaN and ZnO, clearly motivating the presented uniaxial pressure-dependent Raman measurements on bulk AlN crystals.

DOI: [10.1103/PhysRevB.90.205206](https://doi.org/10.1103/PhysRevB.90.205206)

PACS number(s): 78.30.Fs, 78.30.Am, 62.50.–p, 81.40.Vw

I. INTRODUCTION

The continuous progression of AlGaIn-based light emitting diodes and laser diodes towards emission in the deep ultraviolet (UV) spectral range [1] is accompanied by the need for alternative substrates in order to replace the commonly applied GaN, GaN/sapphire [2], and SiC substrates [3]. While these substrates allowed certain advances into the UV spectral range so far, their future application is problematic due to the naturally by heteroepitaxy introduced strain levels and defects [2,4]. As a result, high structural defect concentrations are commonly observed in heteroepitaxially grown films, seriously degrading the material quality [1,5]. AlN substrates appear as most promising alternative for the continuous evolution of nitride-based optical devices towards the deep UV spectral range [6–8]. Consequently, not only the growth of AlGaIn films with a high AlN concentration becomes feasible, but also ultimately homoepitaxial growth of AlN for device applications comes within reach. Hereunto, almost strain-free films grown on bulk AlN with low defect concentrations will fulfill the longterm quest for deep UV emitters finding their numerous applications in optoelectronics, water purification, UV curing, and medical diagnostics [1,9,10].

The ability to directly measure the technologically relevant strain state of any nitride material is one of the key elements for their structural characterization and subsequent device implementation. As a nondestructive and cost-effective technique,

Raman spectroscopy can determine the strain level, if the corresponding phonon deformation potentials (PDPs) are known. So far, a full set of experimentally determined PDPs has been reported for, e.g., GaN [11–13], clearly demonstrating the utility of uniaxial pressure-dependent Raman measurements as the most direct way for a precise PDP determination. A corresponding complete and consistent data set for AlN is still a necessity as a large variance is evident in the PDP values reported so far [14–18]. Based on such fundamental PDPs, one can not only examine the strain in bulk nitride materials by nonresonant macro-Raman spectroscopy [19], but also in nanostructures by means of μ Raman spectroscopy [20]. Most recently, even tip-enhanced Raman spectroscopy [21] was demonstrated for nitrides facilitating strain maps based on PDPs with a lateral resolution well below the diffraction limit.

In this contribution, the phonon pressure coefficients (PPCs) for all zone center optical phonon modes in bulk, wurtzite AlN are reported. By combining Raman measurements under the influence of compressive stress along the c axis with reported data for the hydrostatic pressure coefficients of AlN [22–24], we determine the corresponding PDPs. For the A_1 and E_1 modes, we further directly measure the uniaxial pressure dependence of their LO–TO splittings. Based on density functional theory (DFT) implemented in the SIESTA package we derive the corresponding theoretical values for the PPCs and the uniaxial pressure dependence of the related LO–TO splittings along with further fundamental parameters of wurtzite AlN as, e.g., the Poisson ratio, the elastic stiffness constants, and the Young modulus. We obtain a good agreement between theoretically and experimentally determined

^{*}callsen@tu-berlin.de

PPCs for almost all analyzed Raman modes with some particular deviations. Interestingly, such deviations between the experimental and theoretical phonon pressure coefficients scale with the anisotropy of the Raman modes, clearly rendering uniaxial pressure-dependent Raman *measurements* indispensable. By comparing the three wurtzite materials ZnO, GaN, and AlN we gain further insight into the general scaling behavior of phonon pressure coefficients, directly facilitating the identification of cross-material challenges for commonly applied modeling approaches.

II. EXPERIMENTAL DETAILS

The samples analyzed in this work are single-crystal cubes of state-of-the-art, wurtzite AlN with a lateral length of 2.0 mm. This specimen shape particularly suitable for uniaxial pressure measurements was cut from AlN single crystal wafer material grown by the physical vapor transport method on *N*-polar *c*-plane (000 $\bar{1}$) seeds [25–27]. Polar sample surfaces were polished to an optical finish in order to facilitate a homogenous strain distribution throughout the sample after application of uniaxial stress onto the corresponding *c*-plane surfaces. The room temperature macro-Raman measurements were performed using a DILOR XY 800 triple grating Raman spectrometer with the 514.5-nm line of an Ar²⁺-laser as excitation source. All Raman spectra were recorded in backscattering geometry from an *a*-plane surface, where the *c*-axis of the crystals was perpendicular to the direction of incidence of the laser light and parallel to the direction of the applied uniaxial stress (*c* axis $\perp \vec{k}$, *c* axis $\parallel \vec{p}$). The Raman spectra were collected with a CCD array and calibrated with the spectral lines of a neon gas discharge lamp. All Raman shifts are given in air.

The application of uniaxial stress is generally a technological challenge and special care must be undertaken in order to reach a homogenous strain distribution in the sample [28]. We applied an in-house built pneumatic cylinder-piston system as illustrated in Fig. 1 and mounted this uniaxial pressure apparatus in our Raman setup. The apparatus illustrated in Fig. 1 is identical to the system utilized in Refs. [11,29] for similar measurements on GaN and ZnO. A helium gas supply was connected to the pressure transmission chamber of the uniaxial pressure apparatus via a pressure reducing regulator. The particular choice of helium is not necessary for the applied room temperature measurements but also facilitates low temperature measurements on, e.g., exciton-polaritons in ZnO [30] at a temperature of 2 K. The helium gas pressure in the pressure transmission chamber actuates a steel piston directly towards a movable steel hemisphere, which both were hardened by heating and subsequent rapid cooling in an oil bath. As illustrated in Fig. 2(a), the AlN sample is mounted between the piston and the hemisphere whose facets were also polished to an optical surface quality. Consequently, as soon as a small amount of uniaxial pressure is introduced to the sample, the movable hemisphere automatically slides into a perfect position such that its top facet is aligned parallel to the piston's counterpart. We found that an additional thin layer of sprayed teflon at the sample/steel interfaces further improved the homogeneity of the achievable strain distribution. The experimental success of all these efforts was always confirmed

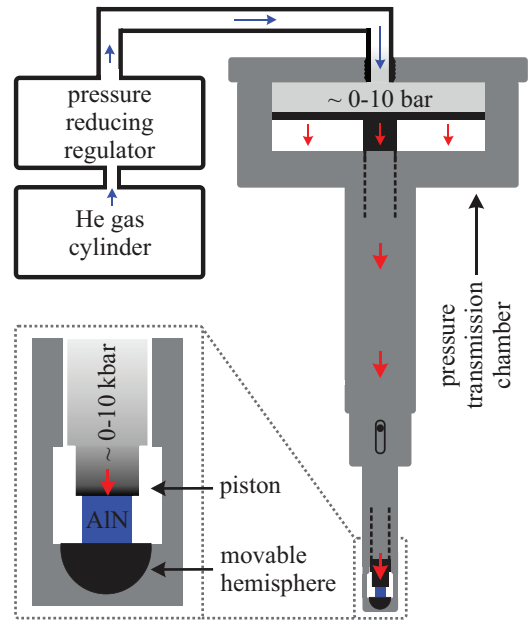


FIG. 1. (Color online) Scheme of the apparatus used for the uniaxial pressure-dependent Raman measurements. The helium gas pressure in the pressure transmission chamber pushes a steel piston onto the wurtzite AlN cube sample that is situated on a movable steel hemisphere. Application of uniaxial pressure allows the hemisphere to slide into the ideal position where all pressure transmitting surfaces are aligned in parallel ensuring a homogenous strain distribution in the sample.

during the measurements by repeating the application and the release of uniaxial pressure for multiple times without the observation of any stress-induced hysteresis. In addition, we always rotated the entire uniaxial pressure apparatus by 180°

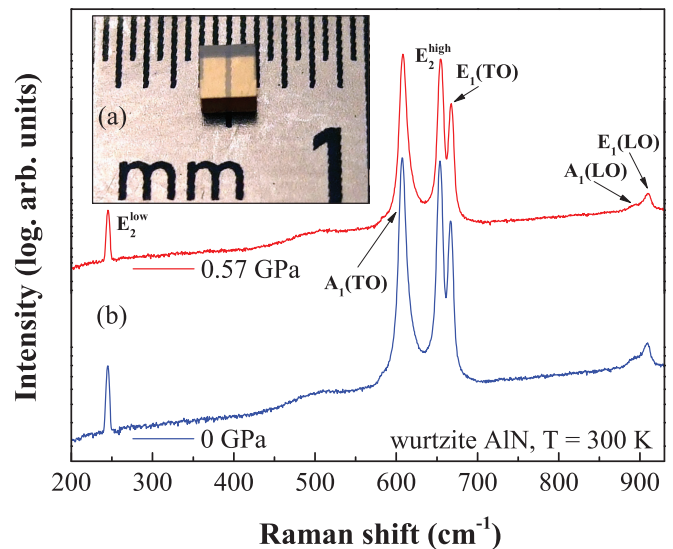


FIG. 2. (Color online) (a) The optically transparent AlN sample analyzed in this work was cut to a cube with a side length of 2.0 mm. All resulting facets were polished to an optical degree. (b) Corresponding Raman spectra for zero and maximal uniaxial pressure recorded in backscattering geometry from an *a*-plane surface of the AlN cube. The uniaxial pressure was applied along the *c*-axis of the crystal.

TABLE II. Comparison of selected experimental values for the phonon deformation potentials a and b (GPa) of all zone center optical Raman modes in wurtzite AlN. The values for a and b are based on different experimental techniques (see Sec. III B) and sample types (bulk crystal - this work, heteroepitaxy - Ref. [14,16,17]). Numbers in parentheses are the errors.

	$-a$			$-b$				
	This work ^a	Ref. [16]	Ref. [17]	Ref. [14]	This work	Ref. [16]	Ref. [17]	Ref. [14]
E_2^{low} :	-116(13)	–	–	–	224(19)	–	–	–
$A_1(\text{TO})$:	952(35)	930(94)	933	–	853(40)	904(163)	721	–
E_2^{high} :	1210(46)	1092(91)	1134	1048	1015(50)	965(161)	1116	1243
$E_1(\text{TO})$:	1273(59)	982(83)	–	–	875(62)	901(145)	–	–
$A_1(\text{LO})$:	606(76)	643(84)	960	–	1052(101)	1157(136)	632	–
$E_1(\text{LO})$:	1012(60)	–	–	–	987(73)	–	–	–

^aIn combination with the results from Ref. [22], see Table I.

As an example, we summarize three Refs. [22–24] in Table I that report rather complete hydrostatic PPC datasets obtained from similar, high-quality bulk AlN material as used in this work. As a result, we can straightforwardly determine three sets of PDPs a and b in Table I for the first-order Raman modes based on the widely accepted C_{ij} values from Ref. [32].

Only the application of the most recent Ref. [22] yields an independent determination of the PDPs a and b for *all* zone center optical Raman modes in wurtzite AlN based on the uniaxial PPCs \tilde{b} , cf. Fig. 3. In addition, this particular PDP data set benefits from the low absolute error intervals reported in Ref. [22] for the hydrostatic PPCs due to the employment of high quality bulk AlN crystals. Such bulk AlN well represents most recent crystal growth advances [25,26,33] and even allows the reproducible application of hydrostatic pressures in excess of 20 GPa [22]. Hence, in order to further compare the obtained PDPs a and b with literature values (Table II), we preferentially rely on the hydrostatic PPC data set of Ref. [22] and consequently avoid any undesired data set intermixing [16]. In comparison, the PDP data set based on Ref. [24] that lacks consideration of the E_2^{low} mode exhibits variations of below 10% for b . However, both LO-modes exhibit a by 14% or even 20% larger PDP a if compared to their counterparts based on Ref. [22], cf. Table I. Generally, the precise determination of the PPCs related to the LO-modes is a challenging task due to their faint signal [22] and/or strong background contributions [23] in wurtzite AlN. Also the $E_1(\text{LO})$ generally suffers and admixture of a small A_1 component [24,34,35] in the backscattering geometry commonly applied for hydrostatic but also uniaxial pressure-dependent measurements resulting in error-prone PPCs. If the data set of Ref. [23] is compared to the PDP results based on Ref. [22] one again only observes variations in excess of 10% for the a value related to the E_2^{low} and the $E_1(\text{TO})$ mode. While the offset for the E_2^{low} mode of 12% can be well understood because of its low overall shift rate, the variation for the $E_1(\text{TO})$ could be related to the close energetic vicinity of the E_2^{high} , possibly affecting a precise peak position determination at elevated hydrostatic pressures due to mode broadening and a resulting merging of the peaks.

B. Comparison of experimental phonon deformation potentials

Table II shows a comparison between already reported, experimental PDP data sets [14,16,17] and the corresponding results from our analysis in Table I based on Ref. [22] and a common set of C_{ij} values [32]. We only list PDPs that

originate from this set of C_{ij} values in order to avoid any further corrections for numerical or systematical errors as discussed by Wagner *et al.* [36]. For the first time, we report the PDPs for the E_2^{low} and $E_1(\text{LO})$ mode within a consistent data set including the values for *all* other zone center optical phonon modes obtained from a wurtzite, bulk AlN crystal. Even though a common set of C_{ij} values forms the basis of the PDP determination, one observes a large variance among so far reported PDP values [14,15,17,18,37,38]. Only the data set reported by Gleize *et al.* [16] reports similar PDP with variations of below 10% with the a value of the $E_1(\text{TO})$ mode as the only exception (23%). Other data sets exhibit larger variations in excess of 10% for the a and b values of, e.g., the E_2^{high} (13% and 22%) [14] and the $A_1(\text{LO})$ mode (58% and 40%) [17], cf. Table II. Consequently, the variance among the reported values originates not only from fluctuations in the overall AlN material quality, but also from the applied experimental techniques. Generally, heteroepitaxy-based approaches [16,18,37,38] and the ball-on-ring technique [14,15,17] seem to provide less resilient PDP values if compared to the direct application of uniaxial and hydrostatic stress to a bulk AlN crystal.

IV. THEORETICAL DETERMINATION OF THE PHONON PRESSURE COEFFICIENTS

For comparative purposes, we did not only measure the PPC \tilde{b} , but also calculated hydrostatic and uniaxial PPCs for all relevant optical phonon modes using the SIESTA software package [39]. SIESTA implements density functional theory to solve the many electron problem applying the generalized gradient approximation (GGA) for the exchange-correlation potential. The valence electrons are represented by numerical atomic orbitals and the core electrons by Trouiller-Martins norm-conserving pseudopotentials [40] with the valence states of N and Al taken as $2s^22p^3$ and $3s^23p^1$, respectively. The default double-zeta plus polarization (DZP) basis sets are used for both atomic species yielding essentially the same results for lattice constants and phonon frequencies as a DZP basis optimized for this system, however, at a slightly smaller computational cost. The most important parameter in the SIESTA calculations is the cutoff radius specified for the atomic orbitals, beyond this cutoff the orbitals are identically zero. To control this cutoff radius with a single parameter for all atoms a confinement energy is specified, by which

TABLE III. Hydrostatic phonon pressure coefficients $2\tilde{a} + \tilde{b}$ ($\text{cm}^{-1}/\text{GPa}$) for wurtzite AlN derived by density functional theory (DFT) in the generalized gradient (GGA) and the local density (LDA) approximation in conjunction with the linear muffin tin orbital method (LMTO). Selected DFT calculations (Ref. [44,45], this work) separately yield \tilde{a} and \tilde{b} ($\text{cm}^{-1}/\text{GPa}$) as also measured for all zone center optical Raman modes (bold, this work). Numbers in parentheses are the errors.

	$-(2\tilde{a} + \tilde{b})$				$-\tilde{a}$			$-\tilde{b}$		
	This work	Refs. [44,45]	Ref. [22]	Ref. [46]	This work	Refs. [44,45]	This work	Ref. [44,45]	This work	Ref. [44,45]
E_2^{low} :	-0.41	-0.05	-0.02	-0.29	-0.34(3)	-0.38	-0.47	0.75(4)	0.35	0.89
$A_1(\text{TO})$:	3.66	3.06	3.83	4.29	1.45(2)	1.37	1.42	1.46(2)	0.92	0.22
E_2^{high} :	4.70	4.21	4.95	4.79	1.87(4)	1.53	1.28	1.66(2)	1.64	1.65
$E_1(\text{TO})$:	4.13	3.79	4.48	4.36	2.07(10)	1.50	1.29	1.20(2)	1.13	1.21
$A_1(\text{LO})$:	3.84	3.57	4.15	—	0.67(21)	1.03	1.11	2.37(19)	1.78	1.35
$E_1(\text{LO})$:	4.01	4.01	4.57	—	1.50(14)	1.39	1.32	1.78(9)	1.23	1.37
Technique :	GGA	LDA	GGA	LDA+LMTO	Exp. ^a	GGA	LDA	Exp.	GGA	LDA

^aIn combination with the results from Ref. [22].

the orbitals are raised due to their confinement. The default value is 20 mRy, which in our experience does not yield well-converged total energies [41]. Instead, we use 5 mRy representing a good compromise between computational time and convergence with total energies converged to better than ~ 0.01 eV. The integrals are evaluated on a real-space grid specified in terms of the maximum energy of a plane-wave that could be represented on this grid. Here, we apply a 1600 Ry grid. The reciprocal space sampling was performed on a $20 \times 20 \times 20$ Monkhorst-Pack grid [42]. Both of these parameters have been deliberately set at a high level in order to give extremely well converged total energies and forces. The phonon frequencies are essentially completely converged with respect to the real-space grid and are converged to $\leq 0.5\%$ with respect to the reciprocal grid. Geometry optimizations of the unit cell and internal relaxation of the atoms are computed up to a tolerance of 0.005 GPa and 0.01 eV/Å.

The phonon frequencies at the zone center are calculated within the frozen phonon method, whereby the dynamical force matrix is determined directly by displacing each atom individually and calculating the resulting forces. In polar materials, such as AlN, the optical modes are split at the Γ point due to the presence of macroscopic fields (see Sec. VI), an effect that is not reproduced by the calculated (analytic) component of the force matrix. The LO-TO splitting was therefore evaluated by calculating the Born effective charge tensor using the geometric Berry phase approach [43]. The pressure-dependent value of the clamped ion dielectric constant (ϵ_∞) is also required in order to evaluate this splitting and here we use the dependence reported by Wagner *et al.* [44].

A summary of the resulting theoretical hydrostatic and uniaxial PPCs is given in Table III along with a direct comparison to the corresponding experimental uniaxial PPCs \tilde{a} and \tilde{b} (bold). In addition Table IV shows further parameters like the Young modulus, the Poisson ratio, etc., that we derive for wurtzite AlN based on our DFT+GGA technique. Note that the calculated C_{ij} values were not used for deriving the PDPs shown in Tables I and II as we prefer to combine the experimental C_{ij} values [32] with our measured PCCs. The overall applicability of the DFT+GGA approach from this work is supported by an additional comparison to theoretical values of hydrostatic PPCs from the literature in Table III. Here, we exemplarily list the results of DFT calculations

based on different approximations, namely GGA (this work and Ref. [22]), LDA [44,45], and LDA in conjunction with the linear muffin tin orbital method (LMTO) Ref. [46]. With an exception for the E_2^{low} mode both DFT+GGA approaches yield equal or larger hydrostatic PPCs if compared to the DFT+LDA technique. However, the PPCs obtained by the second DFT+LDA approach in conjunction with the LMTO method all exceed our own theoretical results, again, with the E_2^{low} mode as the only exception. This particular role of the E_2^{low} mode will be discussed in more detail in Sec. V A along with a direct comparison between theory and experiment focusing on the uniaxial pressure coefficients \tilde{a} and \tilde{b} . Only our calculations and the results by Wagner *et al.* [44,45] allows such a direct comparison as they separately list \tilde{a} and \tilde{b} .

V. DISCUSSION: EXPERIMENT VERSUS THEORY

Generally, we observe a good agreement between the theoretically as well as experimentally derived hydrostatic PPCs $2\tilde{a} + \tilde{b}$ (Tables I and III), and uniaxial PPCs \tilde{a} , \tilde{b} (Table III bold) in wurtzite AlN. However, a few interesting deviations for some particular Raman modes can be noted, e.g., in Table III and will be discussed in the following in addition to general chemical trends.

A. The particular case of the E_2^{low} mode under uniaxial and hydrostatic pressure

Concerning the E_2^{low} Raman mode both theoretical techniques, namely DFT+GGA (this work) and DFT+LDA (Ref. [44,45]), encounter difficulties in predicting the PPCs

TABLE IV. Further parameters of wurtzite AlN obtained from the density functional theory in the generalized gradient approximation applied in this work. The corresponding phonon pressure coefficients are listed in Table III.

$C_{11}, C_{12}, C_{13}, C_{33}, C_{44}$:	361, 130, 93, 339, 107 (GPa)
Poisson ratio:	0.19
Hydr. relaxation coef.:	1.24
Biaxial relaxation coef.:	0.51
Isothermal bulk modulus:	189 GPa
Young modulus:	308 GPa
Biaxial modulus:	489

\tilde{a} and \tilde{b} . While the DFT+GGA approach overestimates $|\tilde{a}|$ for the E_2^{low} mode by 12%, we observe a more striking offset for the DFT+LDA approach. However, for the corresponding $|\tilde{b}|$ of the E_2^{low} mode it is the other way around, here DFT+LDA reaches a fair agreement with an overestimation of 19%, while the DFT+GGA approach predicts a significantly smaller value, cf. Table III.

A similar contradiction between experiment and theory has already been discussed by Manjon *et al.* for the hydrostatic PPC of the E_2^{low} [22]. While a weak hardening of the E_2^{low} is measured (cf. Table I) several DFT approaches consistently predict a mode softening (cf. Table III), clearly underestimating the pressure-induced change of the structural anisotropy in AlN.

The particular matter of the E_2^{low} becomes even more interesting if one compares, e.g., the three material systems ZnO, GaN, and AlN [22,23,47]. For ZnO and GaN the E_2^{low} is softening under the application of hydrostatic pressure in clear contrast to the case of AlN. Calculations reported by Saitta *et al.* [48] allow a better understanding of this context based on the pressure dependence of the shear elastic constant C_{66} that strongly affects the E_2^{low} mode due to its bond-bending nature [22]. Similar to the case of C_{44} , the C_{66} constant is indeed not softening in AlN on the application of hydrostatic pressure up to four times the corresponding wurtzite-to-rocksalt transition pressure, while both elastic constants are indeed softening in GaN and even more rapidly diminishing in ZnO. This scaling behavior directly mirrors the lack of d-electrons in AlN, whose presence in GaN and ZnO is discussed as the origin of the C_{44} and C_{66} softening [48]. Hence despite the rather similar absolute values of the elastic constants in GaN and AlN [32,49], the E_2^{low} mode directly reveals fundamental differences between the nature of the bonds for both material systems, which is also related to a particular effect regarding their phase transition mechanisms [22,48].

Interestingly, based on our uniaxial pressure Raman measurements we can demonstrate that the value of \tilde{b} for the E_2^{low} mode is constant within the error intervals for ZnO, GaN, and AlN [−0.76(5), −0.79(4), and −0.75(4) $\text{cm}^{-1}/\text{GPa}$]. However, the corresponding \tilde{a} values scale from 0.77(3) for ZnO, over 0.55(5) for GaN [11], towards 0.34(3) $\text{cm}^{-1}/\text{GPa}$ for AlN, providing a strong motivation for calculating the uniaxial pressure dependence of the related shear elastic constants. This directly measured scaling behavior does not only nicely match the order of the hydrostatic pressure dependencies of the shear elastic constants in ZnO, GaN, and AlN [48] but also their absolute values that scale from e.g. 40, over 123, towards 131 GPa for C_{66} [32,49,50]. Hence, while the wurtzite crystal structure is stiffening in regard to shear forces from ZnO, over GaN, towards AlN, the overall sensitivity to stress applied perpendicular to the c -axis is naturally decreasing as expressed by the rather small absolute \tilde{a} value of AlN. The resulting high anisotropy of the E_2^{low} mode in AlN (see Sec. V B) is unmatched by any of the other first order Raman modes, apparently evoking challenges in the numerical prediction of the uniaxial pressure dependencies. Additionally, the small absolute PPCs of the E_2^{low} mode in ZnO, GaN, and AlN can be demanding for the considered DFT techniques as overall convergence must be achieved with

sufficiently small error intervals. Concerning uniaxial pressure dependent Raman measurements a similar strong discrepancy between the experimental and theoretical PPCs values for the E_2^{low} mode was already observed for GaN [11]. Here, a DFT+LDA approach underestimated the PPC $|\tilde{b}|$ of the E_2^{low} mode by up to a factor of four [45].

B. General offsets and the Raman mode anisotropy

Putting aside the quite particular behavior of the E_2^{low} mode we can find a more consistent result for all other Raman modes in wurtzite AlN for the PPC \tilde{a} . Both theoretical techniques underestimate $|\tilde{a}|$ for all Raman modes except of the $A_1(\text{LO})$ mode by 5%–26 % (DFT+GGA) and 2%–38 % (DFT+LDA). Solely for the $|\tilde{a}|$ values of the $A_1(\text{LO})$ mode both theoretical techniques yield a strong overestimation by 55% and 67%, cf. Table III. Concerning $|\tilde{b}|$ we observe a good agreement between the measured values and their DFT+LDA counterparts for the E_2^{high} and the $E_1(\text{TO})$ mode but a strong underestimation (23%–85%) for the $A_1(\text{TO})$, $A_1(\text{LO})$, and $E_1(\text{LO})$ mode. For these last three Raman modes, the DFT+GGA approach reaches a fair agreement in regard to the experimental values \tilde{b} with a maximal deviation of 25%–37%. A particularly good agreement between the measured and calculated \tilde{b} values (DFT+GGA or LDA) is found for the E_2^{high} mode, which plays an important role for the stress determination as a generally nonpolar Raman mode [20]. However, the corresponding $|\tilde{a}|$ value of the E_2^{high} mode required for the technologically relevant quantification of biaxial stress is underestimated by 26% (GGA) or 38% (LDA), clearly predicting a falsified Raman mode anisotropy that can be defined based on, e.g., PDPs [16] as $A = |a - b|/(a + b)/2$. In this sense, a similar observation is valid for the most anisotropic mode, the E_2^{low} mode ($A = -1.57$) but also the $E_1(\text{TO})$ ($A = -0.09$) and the $A_1(\text{LO})$ ($A = -0.13$) modes exhibit a rather high anisotropy with $|A| \gtrsim 0.1$ that is apparently not adequately described by the applied DFT techniques. Generally, it appears that the offset between the theoretical and experimental values is scaling with the anisotropy of the individual mode, with the E_2^{low} mode as most prominent example.

C. Chemical trends of the uniaxial phonon pressure coefficients

In Ref. [11], we already discussed the particular behavior of the PPC of the mostly bond-stretching $A_1(\text{TO})$ mode by comparing ZnO and GaN. Now we can add AlN to this comparison, based on Kleinman's [51] internal strain parameter $\zeta = (\alpha - \beta)/(\alpha + \beta)$ containing Keating's [52] valence force field parameters α and β for bond stretching and bond bending, respectively. II-VI materials like cubic ZnS exhibit a softening of the LO/TO singlet modes [53] that can also be observed for the $A_1(\text{TO})$ mode in wurtzite CdS [54] and ZnO [11]. These material systems generally exhibit a rather large internal strain parameter ($\zeta \approx 0.7$), directly expressing a strong sensitivity of their ionic bonds to bending and bond-angle distortions while bond-stretching is difficult to achieve. Materials with a lower bond ionicity exhibit lower ζ values directly altering the subtle rigidity balance of the bonds as it is the case for III-V materials. Hence, e.g., zinc blende AlN and GaN exhibit smaller ζ values of 0.550 and 0.477 as

derived by Wang *et al.* [55] based on first-principle plane-wave pseudopotential calculations.

Generally, the applicability of Keating's valence force field model to nonideal wurtzite materials like ZnO, GaN, and AlN is nontrivial, and already the reduction to just one internal strain parameter ζ implies a strong simplification as discussed by Camacho *et al.* [56]. The generalization of Keating's valence force field model for arbitrary wurtzite crystals directly yields a set of four internal strain parameters, unsuitable for the discussion of general chemical trends. Even though the simplifying idea of an ideal wurtzite structure might partially restore the basic concept implied by α , β , and ζ (i.e., no different sets of bond-stretching and bond-bending constants) it obviously cannot predict general chemical trends as one obtains almost identical ζ values for wurtzite GaN and AlN of ≈ 0.62 [56]. However, we prefer to analyze the origin of the following trends for the Raman modes in these three wurtzite systems by means of limited, but still intuitively accessible terms like bond ionicity and ζ as an in detail understanding would require *ab initio* calculations that manage to predict the pressure dependence of, e.g., the shear elastic constants (see Sec. V A). Interestingly, the following trends that we can extract from our measurements directly support the reduction of ζ from ZnO, over AlN, towards GaN as shown in the following based on two selected, prominent Raman modes.

We choose the uniaxial PPCs \tilde{b} of the $A_1(\text{TO})$ and E_2^{high} Raman mode for the analysis of the chemical trends due to their either mostly bond-stretching or bond-bending nature as well as their low experimental error intervals for the pressure coefficients, cf. Table III. Similar trends can be observed for the other Raman modes, but the trends are partially less pronounced and affected by the error intervals as mostly GaN and AlN only exhibit subtle differences for the PPCs of certain modes [e.g., E_2^{low} , $E_1(\text{LO})$]. From ZnO, over AlN, towards GaN the pressure coefficient of the $A_1(\text{TO})$ is rising from $-0.63(3)$, over $1.46(2)$, towards $2.24(11)$ $\text{cm}^{-1}/\text{GPa}$ in parallel to a decreasing internal strain parameter and bond polarity [47], hence, the vulnerability to bond stretching is increasing. In contrast, the uniaxial PPCs \tilde{b} of the E_2^{high} mode is decreasing from $2.94(8)$, over $1.66(2)$, towards $1.38(10)$ $\text{cm}^{-1}/\text{GPa}$ (ZnO, AlN, and GaN), clearly demonstrating the rising resistance to bond bending and bond-angle distortions. These two opposing scaling behavior for the uniaxial PPCs \tilde{b} of the $A_1(\text{TO})$ and E_2^{high} mode are directly connected to the orientation of the atomic oscillations assigned to the individual mode, which occur either parallel [$A_1(\text{TO})$] or perpendicular (E_2^{high}) to the c -axis and cause their opposing dependence on α and β as expressed by the PPC trends.

VI. UNIAXIAL STRESS DEPENDENCE OF THE LO-TO SPLITTINGS

A direct effect of the ionic nature of the bonding in AlN is the splitting of the A_1 and E_1 modes into their transversal-optical and longitudinal-optical components in the presence of polarity-induced macroscopic electric fields. The resulting LO-TO splitting is directly related to Born's transverse effective charge $(e_T^*)^2 \propto (\omega_{\text{LO}}^2 - \omega_{\text{TO}}^2)$ [23,57], whose hydrostatic pressure dependence exhibits a particular scaling

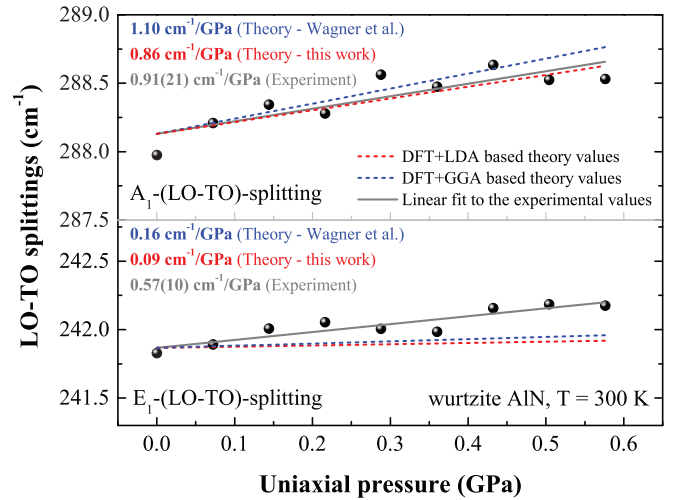


FIG. 4. (Color online) Uniaxial pressure dependence for the LO-TO-splitting of the A_1 and E_1 phonon modes in wurtzite AlN ($\vec{p} \parallel c$ -axis). The solid lines represent linear least-square fits of the data points yielding the LO-TO pressure coefficients and the errors stated in parentheses. Dashed lines show the corresponding theoretically derived uniaxial LO-TO pressure dependence from this work (red) or based on Ref. [44] (blue).

behavior if ZnO, AlN, and GaN are compared [47]. However, the rather small pressure coefficients involved (< 1 $\text{cm}^{-1}/\text{GPa}$) render a precise determination of the pressure dependence of the LO-TO splittings a difficult task and explain the large discrepancies in the literature [22].

Because of the apparent deficiencies in the theoretical description of the overall anisotropy of AlN in regard to \tilde{a} and \tilde{b} as discussed in Sec. V B, we will focus the following comparison between experiment and theory on the *directly* measured LO-TO splittings of the uniaxial PPCs \tilde{b} . Figure 4 illustrates the measured E_1 and A_1 LO-TO splittings under the influence of uniaxial pressure (c -axis $\parallel \vec{p}$) yielding positive pressure coefficients for A_1 : $0.91(21)$ $\text{cm}^{-1}/\text{GPa}$ and E_1 : $0.57(10)$ $\text{cm}^{-1}/\text{GPa}$ based on linear least-square fits to the data points. Such analysis of the uniaxial pressure dependence of mode position differences is only feasible due to the extremely low standard deviation in the entire data set as demonstrated by Fig. 3. For the A_1 LO-TO splitting, we obtain a good agreement between our experimental and theoretical DFT+GGA pressure coefficients as shown in Fig. 4. However, this agreement is only true for the slope of the illustrated theoretical data but not for the intercept that was corrected for all theoretical data sets to match the zero-pressure point of the fit to the experimental data as DFT calculations commonly encounter difficulties in predicting absolute phonon energies and their differences. An underestimation of the slope is observed for the DFT+GGA based prediction of the uniaxial pressure dependence for E_1 LO-TO splitting in regard to the experimental values. The same observation is true for the DFT+LDA approach reported by Wagner *et al.* [44], which breaks down in the case of the E_1 modes but reaches a good agreement for the A_1 modes. However, this agreement is plagued by the already discussed strong offset between the theoretically and experimentally derived values for the PPCs of the $A_1(\text{TO})$ and $A_1(\text{LO})$ mode, cf. Table III.

Concerning the LO-TO splitting of the A_1 mode one observes a scaling of the uniaxial pressure coefficients (pressure $\parallel c$ -axis) from 2.40(42), over 0.91(21), towards $-0.26(29)$ $\text{cm}^{-1}/\text{GPa}$ for ZnO, AlN, and GaN, i.e., in the same order as found for the uniaxial PPCs \tilde{b} of the E_2^{high} and vice versa for the $A_1(\text{TO})$ Raman mode (see Sec. V C). For the corresponding LO-TO splitting of the E_1 mode this scaling behavior is less pronounced as AlN and GaN exhibit within the error intervals identical pressure coefficients [0.57(10) and 0.36(20) $\text{cm}^{-1}/\text{GPa}$] and only ZnO significantly deviates with a negative pressure coefficient of $-0.81(25)$ $\text{cm}^{-1}/\text{GPa}$ in line with the trend reported by Reparaz *et al.* [47] for the case of hydrostatic PPCs. Consistent calculations reporting the uniaxial pressure dependence of the LO-TO splittings related to the A_1 and E_1 mode are needed for all three material systems in order to gain a more detailed understanding of these wurtzite systems and the particular dependence of the Raman modes on the occurring subtle force balances that are selectively altered by the application of uniaxial pressure.

VII. CONCLUSIONS

In summary, we measured the phonon pressure coefficient \tilde{b} for all zone center optical phonon modes in bulk, wurtzite AlN by means of Raman measurements under the influence of uniaxial pressure parallel to the c -axis. In conjunction with the results from hydrostatic pressure-dependent Raman measurements [22–24] we derive all corresponding phonon pressure coefficients \tilde{a} along with a full, consistent set of

phonon deformation potentials relying on experimentally determined stiffness constants C_{ij} [32]. The applied SIESTA implementation of density functional theory yields the theoretical equivalents for the measured pressure coefficients reaching a good agreement with exceptions for some particular Raman modes. Interestingly, the offset between the experimental and theoretical phonon pressure coefficients is scaling with the anisotropy of the particular Raman mode with the E_2^{low} mode as most extreme example. By comparing the three wurtzite materials ZnO, GaN, and AlN we not only reveal general chemical trends for the scaling behavior of uniaxial phonon pressure coefficients but also identify cross-material challenges for the commonly applied modeling approaches. The uniaxial pressure dependence of the LO-TO splitting for the E_1 and A_1 modes was additionally extracted from the experimental data set for AlN. Here, we observe a good agreement with our theoretical results for the A_1 modes but a significant discrepancy for the E_1 modes, thus clearly demonstrating the need for uniaxial pressure-dependent Raman measurements as the most direct technique for determining the phonon pressure coefficients.

ACKNOWLEDGMENTS

This work was supported by the German Research Foundation (DFG) within the Collaborative Research Center (CRC) 787. Partial financial support from NSF (DMR-1108071), DARPA (W911QX-10-C-0027), and ARPA-E (DE-AR0000299) is greatly appreciated.

-
- [1] T. Wunderer, C. L. Chua, Z. Yang, J. E. Northrup, N. M. Johnson, G. A. Garrett, H. Shen, and M. Wraback, *Appl. Phys. Express* **4**, 092101 (2011).
 - [2] M. Kneissl, Z. Yang, M. Teepe, C. Knollenberg, O. Schmidt, P. Kiesel, N. M. Johnson, S. Schujman, and L. J. Schowalter, *J. Appl. Phys.* **101**, 123103 (2007).
 - [3] T. Takano, Y. Narita, A. Horiuchi, and H. Kawanishi, *Appl. Phys. Lett.* **84**, 3567 (2004).
 - [4] A. Zeuner, H. Alves, D. M. Hofmann, B. K. Meyer, A. Hoffmann, G. Kaczmarczyk, M. Heuken, A. Krost, and J. Bläsing, *Physica Status Solidi (b)* **229**, 907 (2002).
 - [5] J. R. Grandusky, S. R. Gibb, M. C. Mendrick, C. Moe, M. Wraback, and L. J. Schowalter, *Appl. Phys. Express* **4**, 082101 (2011).
 - [6] T. Kinoshita, T. Obata, T. Nagashima, H. Yanagi, B. Moody, S. Mita, S.-i. Inoue, Y. Kumagai, A. Koukitu, and Z. Sitar, *Appl. Phys. Express* **6**, 092103 (2013).
 - [7] J. Xie, S. Mita, Z. Bryan, W. Guo, L. Hussey, B. Moody, R. Schlessler, R. Kirste, M. Gerhold, R. Collazo, and Z. Sitar, *Appl. Phys. Lett.* **102**, 171102 (2013).
 - [8] A. Rice, R. Collazo, J. Tweedie, R. Dalmau, S. Mita, J. Xie, and Z. Sitar, *J. Appl. Phys.* **108**, 043510 (2010).
 - [9] W. W. Chow and M. Kneissl, *J. Appl. Phys.* **98**, 114502 (2005).
 - [10] R. Dalmau, B. Moody, R. Schlessler, S. Mita, J. Xie, M. Feneberg, B. Neuschl, K. Thonke, R. Collazo, A. Rice, J. Tweedie and Z. Sitar, *J. Electrochem. Soc.* **158**, H530 (2011).
 - [11] G. Callsen, J. S. Reparaz, M. R. Wagner, R. Kirste, C. Nenstiel, A. Hoffmann, and M. R. Phillips, *Appl. Phys. Lett.* **98**, 061906 (2011).
 - [12] F. Demangeot, J. Frandon, M. Renucci, O. Briot, B. Gil, and R. Aulombard, *Solid State Commun.* **100**, 207 (1996).
 - [13] V. Davydov, N. Averkiev, I. Goncharuk, D. Nelson, I. Nikitina, A. Polkovnikov, A. Smirnov, M. Jacobsen, and O. Semchinova, *J. Appl. Phys.* **82**, 5097 (1997).
 - [14] A. Sarua, M. Kuball, and J. Van Nostrand, *Appl. Phys. Lett.* **81**, 1426 (2002).
 - [15] A. Sarua, M. Kuball, and J. E. Van Nostrand, *Appl. Phys. Lett.* **85**, 2217 (2004).
 - [16] J. Gleize, M. A. Renucci, J. Frandon, E. Bellet-Amalric, and B. Daudin, *J. Appl. Phys.* **93**, 2065 (2003).
 - [17] W. Zhu, A. Leto, K.-y. Hashimoto, and G. Pezzotti, *J. Appl. Phys.* **112**, 103526 (2012).
 - [18] H. J. Trodahl, F. Martin, P. Mural, and N. Setter, *Appl. Phys. Lett.* **89**, 061905 (2006).
 - [19] V. Yu. Davydov, Yu. E. Kitaev, I. N. Goncharuk, A. N. Smirnov, J. Graul, O. Semchinova, D. Uffmann, M. B. Smirnov, A. P. Mirgorodsky, and R. A. Evarestov, *Phys. Rev. B* **58**, 12899 (1998).
 - [20] R. Kirste, R. Collazo, G. Callsen, M. R. Wagner, T. Kure, J. Sebastian Reparaz, S. Mita, J. Xie, A. Rice, J. Tweedie, Z. Sitar, and A. Hoffmann, *J. Appl. Phys.* **110**, 093503 (2011).
 - [21] E. Poliani, M. R. Wagner, J. S. Reparaz, M. Mandl, M. Strassburg, X. Kong, A. Trampert, C. M. Sotomayor Torres, A. Hoffmann, and J. Maultzsch, *Nano Lett.* **13**, 3205 (2013).
 - [22] F. J. Manjón, D. Errandonea, A. H. Romero, N. Garro, J. Serrano, and M. Kuball, *Phys. Rev. B* **77**, 205204 (2008).
 - [23] A. R. Goñi, H. Siegle, K. Syassen, C. Thomsen, and J.-M. Wagner, *Phys. Rev. B* **64**, 035205 (2001).

- [24] M. Kuball, J. M. Hayes, A. D. Prins, N. Van Uden, D. J. Dunstan, Y. Shi, and J. H. Edgar, *Appl. Phys. Lett.* **78**, 724 (2001).
- [25] Z. G. Herro, D. Zhuang, R. Schlessler, R. Collazo, and Z. Sitar, *J. Cryst. Growth* **286**, 205 (2006).
- [26] Z. G. Herro, D. Zhuang, R. Schlessler, and Z. Sitar, *J. Cryst. Growth* **312**, 2519 (2010).
- [27] P. Lu, R. Collazo, R. F. Dalmau, G. Durkaya, N. Dietz, B. Raghathamachar, M. Dudley, and Z. Sitar, *J. Cryst. Growth* **312**, 58 (2009).
- [28] M. Cardona, *Physica Status Solidi B* **198**, 5 (1996).
- [29] M. R. Wagner, G. Callsen, J. S. Reparaz, J.-H. Schulze, R. Kirste, M. Cobet, I. A. Ostapenko, S. Rodt, C. Nenstiel, M. Kaiser, A. Hoffmann, A. V. Rodina, M. R. Phillips, S. Lautenschläger, S. Eisermann, and B. K. Meyer, *Phys. Rev. B* **84**, 035313 (2011).
- [30] M. R. Wagner, G. Callsen, J. S. Reparaz, R. Kirste, A. Hoffmann, A. V. Rodina, A. Schleife, F. Bechstedt, and M. R. Phillips, *Phys. Rev. B* **88**, 235210 (2013).
- [31] T. C. Damen, S. Porto, and B. Tell, *Phys. Rev.* **142**, 570 (1966).
- [32] L. E. McNeil, M. Grimsditch, and R. H. French, *J. Am. Ceram. Soc.* **76**, 1132 (1993).
- [33] J. H. Edgar, L. Liu, B. Liu, D. Zhuang, J. Chaudhuri, M. Kuball, and S. Rajasingam, *J. Cryst. Growth* **246**, 187 (2002).
- [34] F. Demangeot, J. Groenen, J. Frandon, M. A. Renucci, O. Briot, S. Clur, and R. L. Aulombard, *Appl. Phys. Lett.* **72**, 2674 (1998).
- [35] T. Azuhata, T. Sota, K. Suzuki, and S. Nakamura, *J. Phys.: Condens. Matter* **7**, L129 (1995).
- [36] J. M. Wagner and F. Bechstedt, *Physica Status Solidi (b)* **234**, 965 (2002).
- [37] V. Darakchieva, P. Paskov, T. Paskova, J. Birch, S. Tungasmita, and B. Monemar, *Appl. Phys. Lett.* **80**, 2302 (2002).
- [38] T. Prokofyeva, M. Seon, J. Vanbuskirk, M. Holtz, S. A. Nikishin, N. N. Faleev, H. Temkin, and S. Zollner, *Phys. Rev. B* **63**, 125313 (2001).
- [39] J. M. Soler, E. Artacho, J. D. Gale, A. García, J. Junquera, P. Ordejón, and D. Sánchez-Portál, *J. Phys.: Condens. Matter* **14**, 2745 (Nov. 2002).
- [40] N. Troullier and J. L. Martins, *Phys. Rev. B* **43**, 1993 (1991).
- [41] M. J. Ford, R. C. Hoft, and A. McDonagh, *J. Phys. Chem. B* **109**, 20387 (2005).
- [42] H. J. Monkhorst and J. D. Pack, *Phys. Rev. B* **13**, 5188 (1976).
- [43] R. D. King-Smith and D. Vanderbilt, *Phys. Rev. B* **47**, 1651(R) (1993).
- [44] J.-M. Wagner and F. Bechstedt, *Phys. Rev. B* **66**, 115202 (2002).
- [45] J. Wagner and F. Bechstedt, *Appl. Phys. Lett.* **77**, 346 (2000).
- [46] I. Gorczyca, N. E. Christensen, E. L. Peltzer y Blancá, and C. O. Rodriguez, *Phys. Rev. B* **51**, 11936 (1995).
- [47] J. S. Reparaz, L. R. Muniz, M. R. Wagner, A. R. Goni, M. I. Alonso, A. Hoffmann, and B. K. Meyer, *Appl. Phys. Lett.* **96**, 231906 (2010).
- [48] A. M. Saitta and F. Decremps, *Phys. Rev. B* **70**, 035214 (2004).
- [49] A. Polian, M. Grimsditch, and I. Grzegory, *J. Appl. Phys.* **79**, 3343 (1996).
- [50] T. Azuhata, M. Takesada, T. Yagi, A. Shikanai, S. Chichibu, K. Torii, A. Nakamura, T. Sota, G. Cantwell, D. Eason, and C. Litton, *J. Appl. Phys.* **94**, 968 (2003).
- [51] L. Kleinman, *Phys. Rev.* **128**, 2614 (1962).
- [52] P. N. Keating, *Phys. Rev.* **145**, 637 (1966).
- [53] M. Siakavellas, A. Kontos, and E. Anastassakis, *J. Appl. Phys.* **84**, 517 (1998).
- [54] R. J. Briggs and A. K. Ramdas, *Phys. Rev. B* **13**, 5518 (1976).
- [55] S. Q. Wang and H. Q. Ye, *Physica Status Solidi (b)* **240**, 45 (2003).
- [56] D. Camacho and Y. M. Niquet, *Physica E* **42**, 1361 (2010).
- [57] P. Y. Yu and M. Cardona, *Fundamentals of Semiconductors*, 4th ed. (Springer, Heidelberg, 2010).